J. metamorphic Geol., 1995, 13, 687–700

Andalusite-bearing veins at Vedrette di Ries (eastern Alps, Italy): fluid phase composition based on fluid inclusions

B. CESARE[1] AND L. S. HOLLISTER[2]
[1] Dipartimento di Mineralogia e Petrologia, Università di Padova, I-35137 Padova, Italy
[2] Department of Geological and Geophysical Sciences, Princeton University, Princeton, NJ 08544, USA

ABSTRACT Andalusite-bearing veins formed during contact metamorphism in the aureole of the Vedrette di Ries tonalite. In the veins, quartz crystals that are completely armoured by andalusite or that occur in strain shadow areas contain three generations of fluid inclusions: low-salinity H_2O–CO_2–CH_4 mixtures with $CH_4/(CO_2 + CH_4) \leq 0.35$ (type A); low-salinity aqueous fluids (type B); H_2O-free, CO_2–CH_4 fluids with the same carbonic speciation as A (type C). Carbonic types A and C typically have a dark appearance, which is attributed to graphite coatings on inclusion walls. Microstructural analysis of the host quartz and calculated densities indicate that type A inclusions were likely trapped during vein formation. These inclusions underwent strain-assisted re-equilibration during cooling that resulted in density increases without change of composition. After the rocks had cooled below about 350° C, type C inclusions appear to have formed from one of the immiscible fractions after unmixing of the H_2O–CO_2–CH_4 fluid mixtures. Aqueous type B inclusions, apparently trapped between 225 and 350° C, could represent an independent fluid, or could be the H_2O-rich fraction of unmixed type A fluids. Taking account of the uncertainties, the composition and density of the complex type A inclusion fluids are in good agreement with the properties of primary fluids calculated from the petrological data. The fluid inclusion data support the model of vein formation by hydrofracturing as a result of dehydration of graphitic metapelites. These new results also demonstrate the importance of considering strain in the interpretation of metamorphic fluid inclusions.

Key words: andalusite veins; C–O–H system; fluid inclusions; Italian eastern Alps; re-equilibration.

INTRODUCTION

The mechanisms by which mass transport and mineral deposition take place in veins containing Al_2SiO_5 polymorphs are particularly enigmatic because the solubility of Al_2SiO_5 in aqueous fluids is exceedingly low compared to most other chemical species. As a consequence, large amounts of metasomatic fluids have been proposed to have passed through host rocks in order to carry the alumina to form the kyanite or andalusite in the veins (e.g. Yardley, 1986; Kerrick, 1988). Such massive fluid flow implies that fluids were externally derived and may have been out of equilibrium with the host rocks. As a consequence, a metasomatic origin for deposition of the aluminium silicates, possibly promoted by alkali-chloride-rich solutions, is generally considered the most reasonable mechanism for the genesis of Al_2SiO_5-bearing veins (Kerrick, 1990). Conversely, the study of the andalusite-bearing veins at Vedrette di Ries (Cesare, 1994a) led to a closed-system genetic model where veins formed as a result of pelite dehydration during contact metamorphism. In this model, after veins were opened by hydrofracturing, the aluminium silicate components diffused through the grain boundary fluid from the reaction sites where they were produced to nucleation sites on the walls of the fluid-filled cavities. Necessary conditions for this model are that fluid pressure at the time of mineral growth in veins equalled lithostatic pressure, and that the composition of the vein-forming fluid was the same as that of the metapelitic host-rock.

The objective of the present study was to see if we could identify in fluid inclusions the fluid that was present when the vein was formed and to compare this fluid with that predicted by Cesare (1994a). If the composition and density of the vein-forming fluid were similar to the properties calculated for the synmetamorphic fluid, then the model of metasomatizing fluids for the Vedrette di Ries occurrence could be eliminated.

GEOLOGICAL SETTING

The Vedrette di Ries pluton is a granodioritic to tonalitic intrusive of Oligocene age, which was emplaced in the Austroalpine basement of the eastern Alps, south of the Tauern Window (Fig. 1). In this area, the country rocks of the pluton are mainly composed of metapelites and metapsammites, with minor amphibolite and pegmatitic orthogneiss layers; these rocks were part of the palaeo-African continental crust which was later involved in the formation of the Alpine chain. The polymetamorphic evolution of the Austroalpine basement south of the Tauern Window has been summarized by Stökhert (1982), Becker *et al.* (1987) and Frank *et al.* (1987). For the purpose of this study it is relevant to note that the Oligocene contact metamorphism is the last metamorphic episode recorded in the area, and that the contact aureole

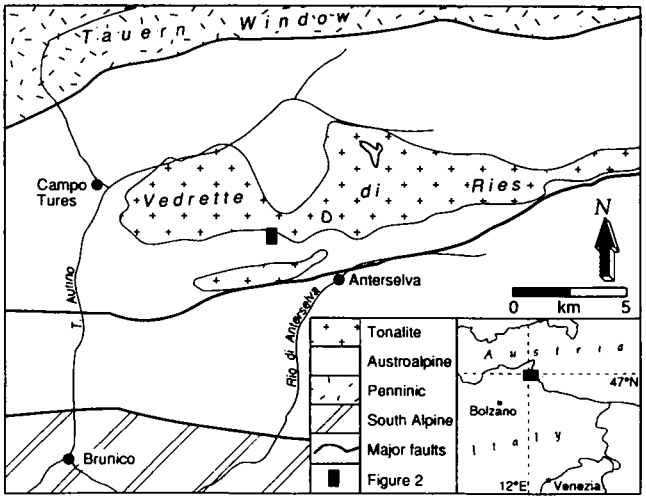

Fig. 1. Geological sketch map of the Vedrette di Ries intrusive and adjacent metamorphic units (after Borsi *et al.*, 1978).

developed in rocks that had already been partly dehydrated during pre-Alpine and Alpine regional metamorphic events.

Based on phase equilibria in the metapelitic lithologies (Cesare 1992, 1994b), the *P–T* path of contact metamorphism consisted of rapid heating from about 350 ± 50° C to maximum temperatures of 600–650° C, followed by cooling to the initial temperature. The heating–cooling pulse occurred at pressures in the range 2.5–3.75 kbar.

Andalusite-bearing veins occur only within the aureole, within 1 km of the intrusive contact. They contain andalusite, quartz and biotite in variable amounts, and all are hosted by andalusite-bearing metapelitic schists and hornfelses. Veins are subvertical, perpendicular or at a high angle to the S-dipping main penetrative foliation of host-rocks; this foliation developed during Alpine deformation (Stöckhert, 1982; Mager, 1985), before the emplacement of the intrusive. Veins are planar and parallel-sided, with tapered terminations; very rarely are they thicker than 3–4 cm. Veins are generally isolated, and do not form interconnected networks; they show little or no evidence of strain at the outcrop scale, with only minor shear along surfaces parallel to their walls. The andalusite-bearing veins, as well as other discordant veins, occur in only minor abundance (<1% of the outcrop area) in the aureole. A detailed field and petrographic study of andalusite-bearing veins and their host rocks was given by Cesare (1994a), who concluded that the veins formed during the contact metamorphism as a result of hydrofracturing induced by dehydration reactions occurring in the metapelites. Given the size, shape and occurrence of the veins, the strong control of host-rock mineralogy on the vein assemblage, and the lack of any evidence of hydrothermal activity in the aureole, Cesare (1994a) proposed that a locally derived fluid entered the veins during hydrofracturing, and that andalusite grew as a result of a mass-transport mechanism dominated by diffusion through the fluid from the host schists to the veins. The diffusion medium and vein-filling fluid was produced mainly by chlorite dehydration that accompanied andalusite growth in the host-rocks; because graphite is present in the metapelites, the fluid should consist of a C–O–H mixture in equilibrium with graphite at the pressure and temperature conditions of vein formation.

SAMPLE DESCRIPTION AND MICROSTRUCTURES

The macroscopically least deformed or altered samples of andalusite-bearing veins were chosen in order to maximize the chance for the preservation of primary fluid inclusions. The five samples selected for fluid inclusion studies were collected at two outcrops that are particularly rich in veins and occur in two different metamorphic zones of the aureole (Fig. 2). Samples VR489b1 and VR489b2 belong to 'outcrop 1' of Cesare (1994a). This outcrop is located about 800 m from the tonalite and occurs in the andalusite–staurolite zone of the contact metamorphism. In this area, veins are considered to have developed close

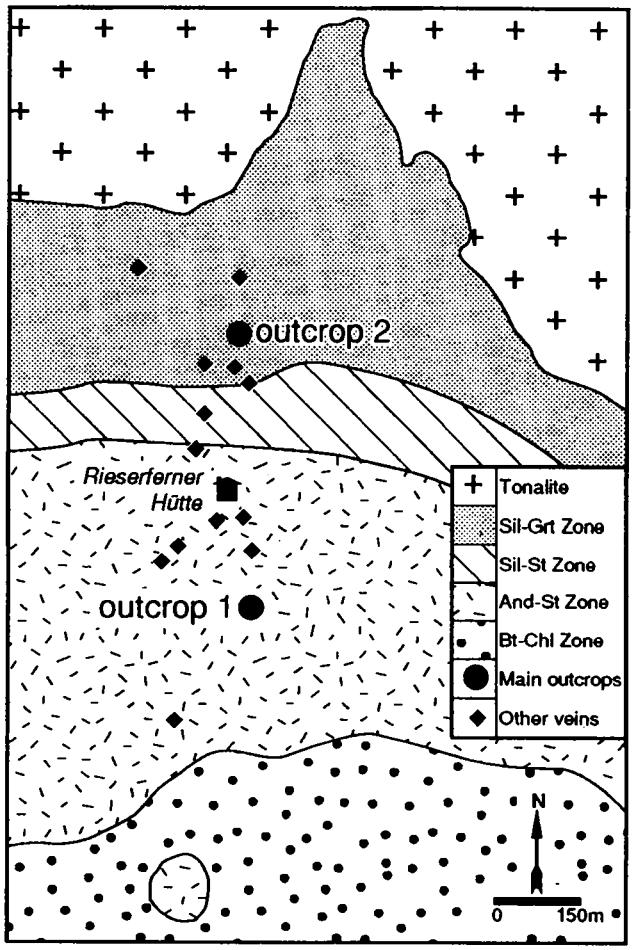

Fig. 2. Location of studied outcrops and of andalusite vein occurrences in the southern Vedrette di Ries aureole. Mineralogical zones of contact metamorphism after Cesare (1992).

Table 1. Location, size and modal composition (visual estimate) of analysed vein samples.

Sample no.	Location	Vein length (m)	Vein thickness (cm)	Mineralogy
VR489b1	Outcrop 1	0.8	1.5	Qtz70–And25–Bt5
VR489b2	Outcrop 1	0.3	1.5	Qtz15–And75–Bt10
VR357	Outcrop 2	4	5.0	Qtz75–And25
VR471	Outcrop 2	2	3.0	Qtz55–And40–Bt5
VR650	Outcrop 2	0.3	1.5	Qtz15–And65–Bt15–Sil5

to peak temperature conditions, with no additional heating after their formation. Samples VR357, VR471 and VR650 occur at 'outcrop 2', 150 m from the contact. Microstructural analysis suggests that after formation of the veins in the stability field of andalusite, veins and host-rocks at outcrop 2 underwent higher temperatures which produced the AFM assemblage garnet–biotite–sillimanite (+muscovite + quartz). Evidence for this prograde continuous heating consists of partial pseudomorphs of sillimanite after andalusite, both in veins and host-rocks. Data on location, size and mineralogy of the various samples are summarized in Table 1.

Quartz, andalusite and biotite are unevenly distributed within veins: andalusite and biotite are located close to vein walls, in polycrystalline clusters, whereas quartz is concentrated mainly in the central parts. Mineral grain size is variable, generally increasing from vein walls to cores. Andalusite crystals may be up to 3 cm in length in the thicker veins. The andalusite content of veins is highly variable; in places andalusite makes up to 80% of the vein's volume (VR489b2, VR650). Biotite is abundant in veins only if host-rock garnet is replaced by biotite.

As shown by quartz textures, various degrees of strain affected each vein sample; mechanical behaviour appears to be influenced by the relative amounts of quartz, andalusite and biotite within veins. In quartz-rich veins (VR489b1, VR357, VR471), strain (essentially shearing parallel to vein walls) is accommodated by undulose extinction and minor subgrain formation in quartz (Fig. 3a), and by bending of biotite (when present). In these veins, coarse andalusite (that can contain quartz inclusions, Fig. 3b) behaves as a rigid object, and strain shadows where quartz is practically undeformed occur adjacent to the larger andalusite crystals or within andalusite clusters (Fig. 3c). Other sites where unstrained quartz occurs are located at some undeformed vein walls, especially if a thin layer of biotite is present to accommodate deformation (VR489b1). Conversely, when andalusite fills most of the vein and has a finer grain size (VR489b2, VR650), strain cannot be partitioned through the rare, dispersed quartz grains. This results in a weak but diffuse deformation of the whole vein aggregate, in which andalusite acts as the matrix mineral. Thus, in these samples, most quartz grains apparently armoured within andalusite clusters are also slightly strained and show undulose extinction and deformation bands.

Deformation was accompanied by retrogression and hydration of vein minerals: 'shimmer aggregates' of fine-grained white mica after andalusite, and chlorite after biotite are locally present. Hydration phenomena are concentrated at sheared vein borders.

Because all the fluid inclusion samples show similar textural and chemical features, the following description, unless otherwise noted, refers to aspects that are common to the andalusite-bearing veins. Fluid inclusions of sufficient size for microthermometry (10–20 μm) only occur in quartz; abundant inclusions in andalusite are too small (<3 μm) for microthermometry. Three distinct types of fluid inclusions have been distinguished on the basis of their apparent composition at room temperature (21° C): two- or three-phase water-carbonic inclusions (A), two-phase aqueous inclusions (B), and one- or two-phase carbonic inclusions (C). The various types generally occur at separate sites within quartz; if inclusions of more than one type coexist, they are located in a different microstructural position. Inclusions of all types can have both irregular or euhedral negative crystal shape within the same site. A distinctive feature common to many carbonic inclusions of both types A and C is a dark appearance (Fig. 3d). Some inclusions are completely black, but their behaviour in the heating–cooling stage is the same as adjacent clearer inclusions: during cooling, the white CO_2 solid suddenly forms at about −95° C, indicating that inclusions are neither empty nor solid. Similar carbonic dark inclusions are described by Roedder (1984, p. 526) and Morgan *et al.* (1993), who, respectively, suggested and proved graphite to be present as a thin layer coating the inclusion walls.

Inclusions in quartz can occur in several textural settings: isolated or in small groups with random distribution, in planar arrays, and in trails. Isolated inclusions and clusters are typical of quartz grains that are included in poikilitic andalusite (Fig. 3e) or completely surrounded by andalusite aggregates (Fig. 3f). In this type of microstructure, quartz is generally strain-free, with notable exceptions in the andalusite-rich vein samples (e.g. VR489b2, Fig. 3g). Planar or linear distributions occur in slightly more deformed quartz and in the high-strain areas of veins, where inclusions usually form parallel sets that cross-cut grain boundaries. Planes of fluid inclusions can also be present in zones of unstrained quartz, but in this case they are limited to a single grain. Aqueous-carbonic inclusions of type A are mainly isolated or in small groups in the strain-free or low-strain quartz grains (Fig. 3h); rarely are they distributed along trails, but in such cases they do not cross grain boundaries (Fig. 3i). Carbonic inclusions without visible water (type C) are present in the same settings as type A, but in slightly more deformed quartz grains. They also form secondary planes (Fig. 3j) sometimes cross-cutting grain boundaries. Aqueous inclusions of type B are always found in planes (often in parallel sets, Fig. 3k,l) in the areas of higher deformation. When they occur with type B inclusions, carbonic and aqueous inclusions are located in different planes.

The combination of textural and compositional observations provide a preliminary trapping sequence. The isolated type A inclusions (and the small groups as well) within unstrained quartz could represent the inclusions trapped during vein formation, and therefore they may contain the fluid present at that time. A similar history can

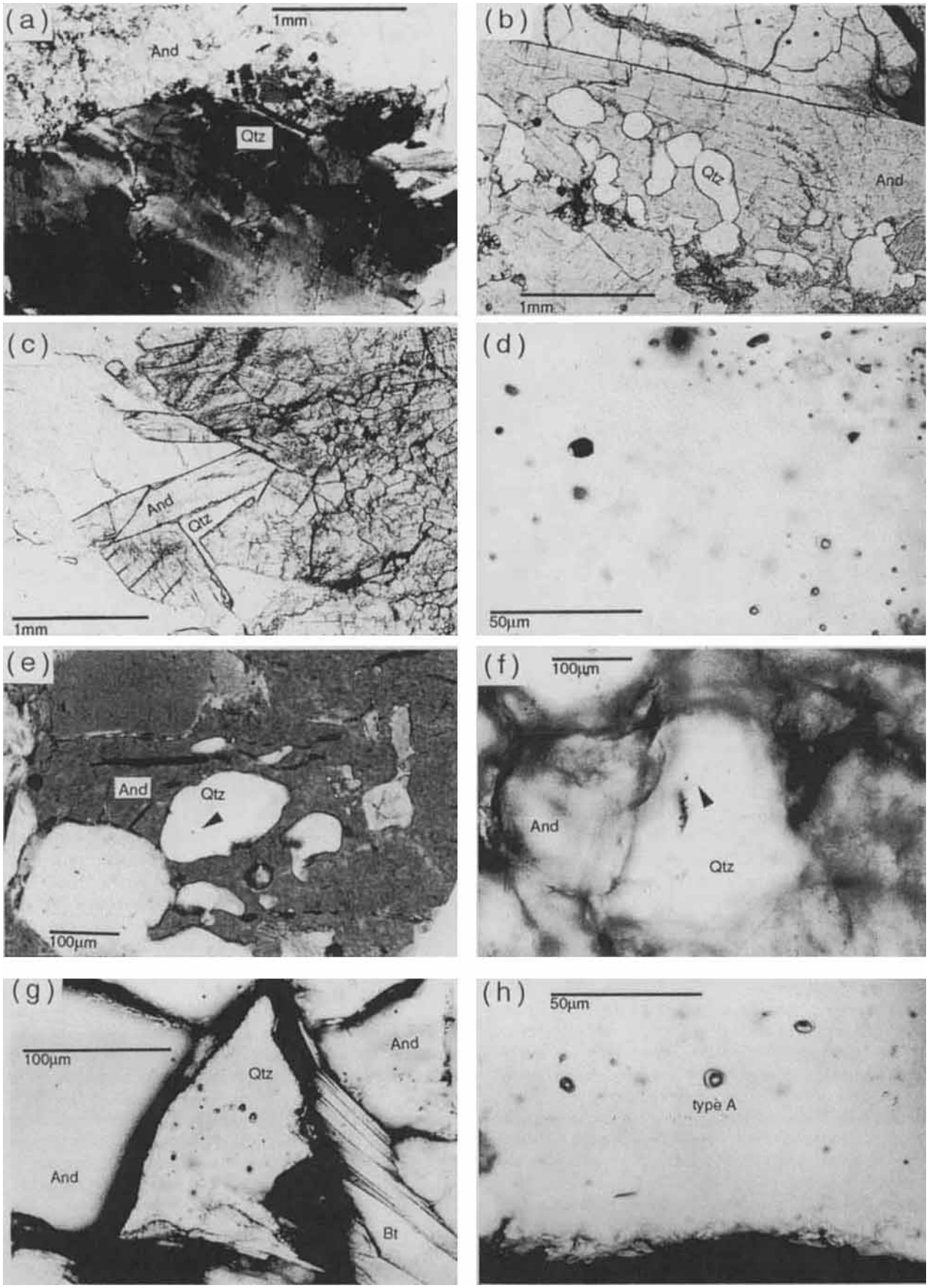
(a)
1mm
And
Qtz
(b)
Qtz
And
1mm
(c)
And
Qtz
1mm
(d)
50μm
(e)
And
Qtz
100μm
(f)
100μm
And
Qtz
(g)
100μm
Qtz
And
And
Bt
(h)
50μm
type A

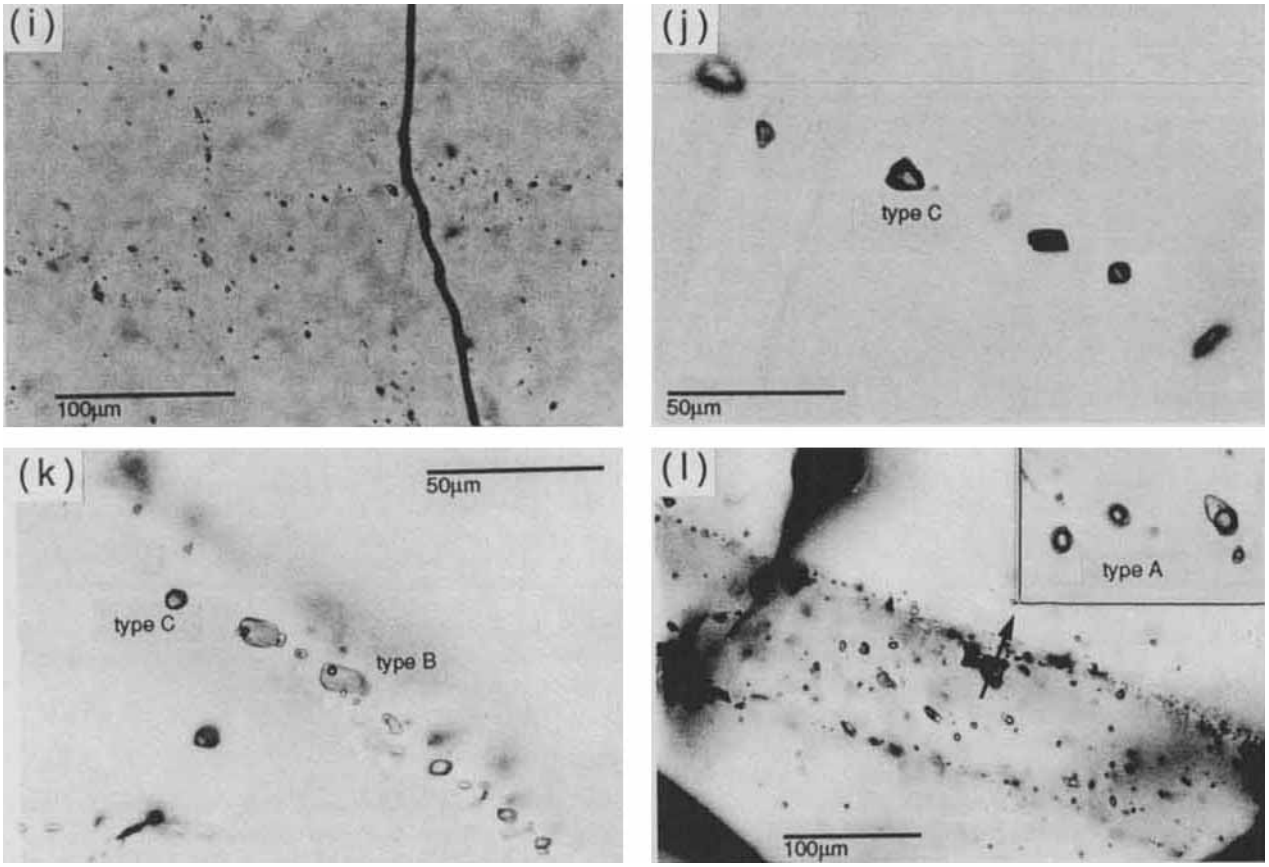

Fig. 3. Quartz microstructures and fluid inclusion occurrences in andalusite-bearing veins. (a) Fine-grained andalusite aggregate (top) adjacent to a large, strained quartz crystal showing deformation bands and incipient subgrain formation. The quartz crystal contains abundant planes and trails of fluid inclusion, shown in (l) (VR489b2). (b) Quartz grains included in a coarse andalusite crystal. (c) Undeformed quartz embedded within andalusite cluster. (d) Two-phase (H_2O-rich liquid + carbonic liquid) type A inclusions; some of them are very dark (VR471). (e) Isolated fluid inclusion (arrow), in a quartz grain within poikilitic andalusite (VR650). (f) Isolated inclusions in unstrained quartz armoured by andalusite (VR471). (g) Two-phase type A inclusions in a quartz grain armoured by andalusite and biotite. In this example, the quartz host appears to be weakly strained (VR489b2). (h) Two-phase type A inclusions in unstrained quartz. This site was preserved from strain by a large andalusite crystal (black, bottom) (VR471b). (i) Intersecting planes of type A inclusions within weakly strained quartz (VR357). (j) Negative crystal, one-phase (carbonic liquid) type C inclusions along a trail (VR489b1). (k) Plane of two-phase (H_2O-rich liquid + H_2O-rich vapour) type B inclusions, and adjacent isolated one-phase inclusions of type C (VR489b1). (l) A few, isolated type A inclusions (enlarged on top right) between parallel planes of two-phase type B (VR489b2).

be envisaged for the isolated type C inclusions, although these mainly occur in slightly more deformed quartz (particularly in the andalusite-rich veins VR650). Inclusions of type B and some of type C have clearly developed in a later stage, after the veins were completely formed.

MICROTHERMOMETRY

Temperature measurements were obtained for ≈300 inclusions from doubly polished, 200-μm-thick chips, using a USGS type heating–freezing stage (made by FLUID Inc.) at the Department of Geological and Geophysical Sciences of Princeton University. Stage calibration at −56.6, 0.0 and 374.1° C was performed using natural and synthetic pure CO_2 and H_2O standards. A heating rate of 2° C/min was adopted during analysis in the interval −63 to 31° C; in the same range, duplication of measurements within ±0.2° C could be obtained.

Temperatures were determined for the following phase transitions: final melting of CO_2 ($T_m^{CO_2}$), final melting of H_2O (T_m^{ice}), final melting of clathrate (T_m^{cla}), homogenization of CO_2 ($T_h^{CO_2}$) and final homogenization of water–carbonic inclusions (T_h^f). Because of the very small inclusion dimensions and their dark aspect, it was difficult to observe the behaviour of clathrates and to determine the precise volume of the carbonic fraction within type A inclusions. Reliable measurements of T_m^{cla} are thus scarce. Given the quite high density of the inclusions and the possibility of their decrepitation upon heating, T_h^f values of type A and B inclusions were measured in only a few chips.

Microthermometric results are summarized in Table 2. All samples show a similar behaviour for the three inclusion types, so a general description can be made.

Table 2. Microthermometric data and estimated chemical/volumetric parameters of representative type A, B and C fluid inclusions. *Measured only in a few inclusions, to avoid extensive decrepitation.

Sample	No.	Type	$T_m^{CO_2}$ (°C)	$T_h^{CO_2}$ (°C)	Homog. type	T_m^{ice} (°C)	T_m^{cla} (°C)	T_h^{f*} (°C)	Vol.% H2O	X_{H_2O}	X_{CO_2}	X_{CH_4}	X_{NaCleq}	Density (g/cm^3)	$CH_4/(CH_4+CO_2)$
VR489b1	1	A	−58.8	18.0	L	−10.1	8.5		40	0.72	0.24	0.04	0.007	0.90	0.13
	2	A	−60.0	0.4	L	−5.0	8.5		40	0.65	0.29	0.05	0.009	0.97	0.17
	3	B				−7.5	8.0		100				0.037	0.93	
	4	B				−8.3			100				0.041	0.95	
	5	C	−59.7	8.8	L				0		0.75	0.25		0.55	0.25
VR489b2	1	A	−61.9	−1.1	L	−8.6	5.7	315	60	0.84	0.10	0.04	0.024	1.02	0.28
	2	A	−63.7	−30.0	C	−9.9	6.0		40		out of Heyen *et al.*'s range				≈0.35
	3	B				−8.1		225	100				0.040	0.94	
	4	B				−8.8	3.0	220	100				0.043	0.95	
	5	C	−58.8	−3.5	L				0		0.90	0.10		0.84	0.10
	6	C	−58.3	15.8	L				0		0.91	0.09		0.65	0.09
VR357	1	A	−59.0	21.6	L	−5.1	7.0	330	60	0.86	0.10	0.02	0.020	0.95	0.15
	2	A	−58.9	17.5	L	−5.0	6.1		60	0.81	0.15	0.02	0.015	0.96	0.12
	3	B				−4.8		232	100	0.97			0.025	0.89	
	4	C	−59.5	−10.5	L				0		0.86	0.14		0.85	0.14
VR471	1	A	−59.1	18.8	L	−8.0	6.0		40	0.70	0.24	0.04	0.017	0.91	0.14
	2	A	−58.8	13.5	L	−3.5	6.9		40	0.70	0.25	0.04	0.013	0.92	0.13
	3	A	−59.5	2.0	L		6.2		40	0.65	0.28	0.05	0.020	0.97	0.14
	4	B				−5.4			100				0.027	0.91	
	5	C	−59.0	14.7	L				0		0.87	0.13		0.61	0.13
	6	C	−59.1	2.5	L	0.0			0		0.88	0.12		0.74	0.12
VR650	1	A	−57.3	25.0	L		6.2		40	0.71	0.26	0.01	0.010	0.86	0.04
	2	A	−57.4	1.6	L				30	0.52	0.44	0.02	0.020	0.96	0.04
	3	B				−4.9			100				0.025	0.90	
	4	C	−57.8	5.2	L				0		0.95	0.05		0.84	0.05

Type A inclusions

All aqueous-carbonic inclusions show a depression of the final melting temperature of CO_2 ($T_m^{CO_2}$, Figs 4 & 5) below −56.6° C, to minimum values of −63.7° C in sample VR489b2. The carbonic fraction of type A inclusions is thus likely to be a mixture of CO_2 and dilutants such as CH_4 or N_2. The average $T_m^{CO_2}$ is between −59 and −60° C, but temperatures vary in each sample within a maximum range of 3° C.

The carbonic fraction of all inclusions homogenizes to the liquid (L + V → L), except for some rare cases of critical homogenization ('fading meniscus') in samples VR489b2, VR471 and VR650. Only two inclusions homogenized to the vapour phase (L + V → V). Critical homogenization phenomena occur in each sample at the maximum $T_h^{CO_2}$ values for a given range of $T_m^{CO_2}$. $T_h^{CO_2}$ values are generally higher than +10° C, and they generally cluster in one or more narrow ranges within each sample. Maximum values of $T_h^{CO_2}$ are inversely correlated with $T_m^{CO_2}$ (Fig. 5), as can be predicted by the behaviour of phase boundaries in the system CO_2–CH_4 (Hollister & Burruss, 1976).

The aqueous part of type A inclusions is generally around 30–60 vol.%. It contains dissolved salts, as indicated by the depression of the final melting temperature of ice (T_m^{ice}), which occurs in the range −11 to −3.5° C (Fig. 6). In most samples, the initial melting of ice occurs at −21° C; in one sample a temperature of −40.4° C was measured. This implies the presence of additional dissolved salts (e.g. $CaCl_2$) besides NaCl. Clathrate hydrates were also observed within type A inclusions. Their presence is indicated by a melting episode between +3 and +9.5° C (Fig. 7). Most clathrate melting episodes take place in the presence of both liquid and vapour CO_2. The carbonic and aqueous liquids of a few type A inclusions could be homogenized to a single phase: this occurred at a final homogenization temperature (T_h^f) of about 300–330° C, with the disappearance of the carbonic bubble. Many inclusions of the same type decrepitated at <300° C, before homogenization.

Type B inclusions

Two-phase aqueous inclusions, which are always located in secondary planes or trails, contain dissolved salts, as indicated by the values of T_m^{ice} in the range −10 to −5° C. These values are in the same range as those of type A inclusions, suggesting a possible genetic relationship between the two families. A few type B inclusions from samples VR489b1 and VR489b2 showed melting at +8 and +3° C: this can be attributed to the melting of clathrate, which would indicate the presence of a small, miscible carbonic fraction in the aqueous fluid. The aqueous inclusions that have been tested for homogenization (samples VR489b2 and VR357, as for the type A ones), show a maximum T_h^f of 225–230° C.

Type C inclusions

The behaviour of optically H_2O-free carbonic inclusions is similar to the carbonic fraction of type A inclusions in the same sample, with $T_m^{CO_2}$ values in the same range (Fig. 4). However, $T_h^{CO_2}$ is generally lower than in H_2O-bearing inclusions, and shows a larger spread (Fig. 5). All type C inclusions homogenize to the liquid phase (L + V → L).

A few type C inclusions from samples VR489b1 and VR471 show evidence for the presence of clathrates and/or ice (Figs 6 & 7). Also, T_m^{ice} and T_m^{cla} measured in these inclusions are in the same range as type A values. The presence of clathrate or ice indicates that at least some inclusions of type C contain H_2O; the H_2O would form a thin film coating the inclusion walls that would be virtually invisible under the microscope.

There is no correlation between microthermometric results and shape of inclusions in both types A and C:

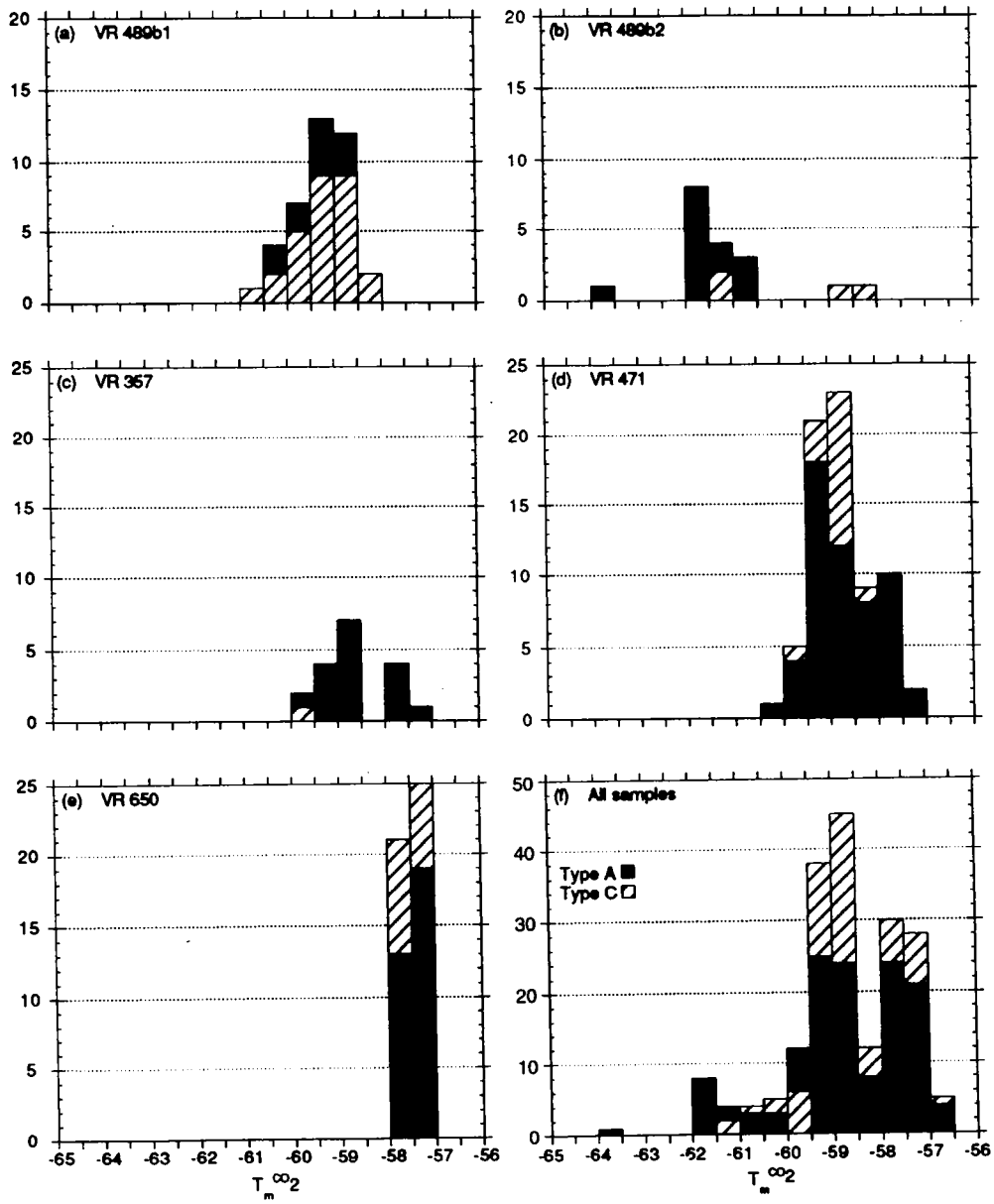

Fig. 4. Individual sample (a–e) and cumulative (f) histograms of $T_m^{CO_2}$ for type A and type C inclusions. All the samples show a depression of the final melting temperature of CO_2 (see also Fig. 5), and, with the exception of sample VR489b2, a similar temperature range for type A and C inclusions.

irregular and negative crystal inclusions show phase transitions at the same temperatures.

FLUID COMPOSITION IN THE SYSTEM C–O–H–NaCl

The sequences and temperatures of phase transitions, observed in all inclusion types of andalusite-bearing veins, can be modelled in the system C–O–H–NaCl or subsets of it (Table 2). At common metamorphic P–T conditions this system comprises the species H_2O (salt solution), CO_2, CH_4 and C (graphite). Laser Raman spectroscopy investigation on some representative inclusions has confirmed the presence of CH_4 in the vapour phase (D. Winslow, pers. comm., 1994).

When dealing with the full C–O–H–NaCl system, quantitative interpretation of compositional and volumetric data from microthermometry alone suffers from several uncertainties and difficulties, mainly arising from: (a) the scarcity of experimental data; (b) the presence of clathrates and their effects on the estimate of X_{CH_4} and bulk salinity, and (c) the sometimes large uncertainty in the visual estimate of vol.% H_2O in the inclusions (Roedder, 1979). Detailed discussion of these problems is beyond the scope of this study, and will be addressed only in part in the description of type A inclusions. Conversely,

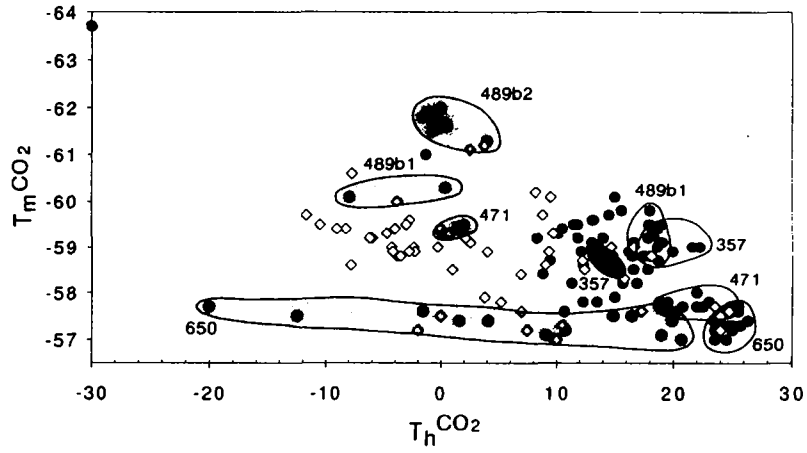

Fig. 5. Cumulative $T_m^{CO_2}$ vs. $T_h^{CO_2}$ diagram. Solid circles: type A; empty diamonds: type C. Empty areas: data clusters from strain-free or low-strain domains; shaded areas: data from strained domains.

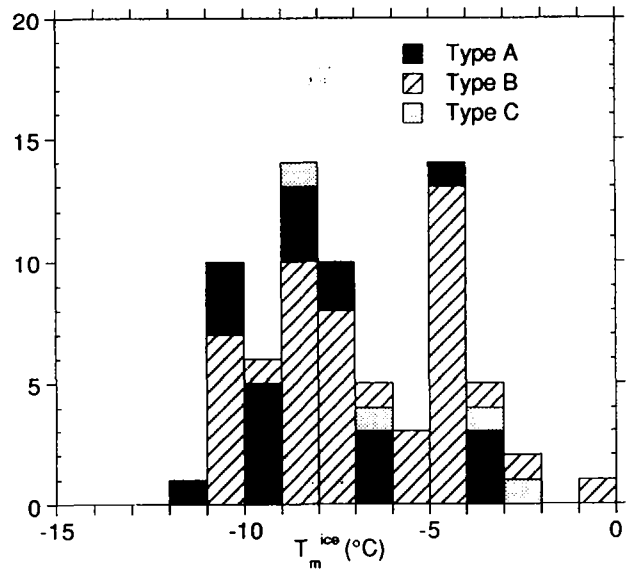

Fig. 6. Cumulative histograms of T_m^{ice}. Ice melting episodes in some inclusions of type C indicate the presence of optically undetected H_2O.

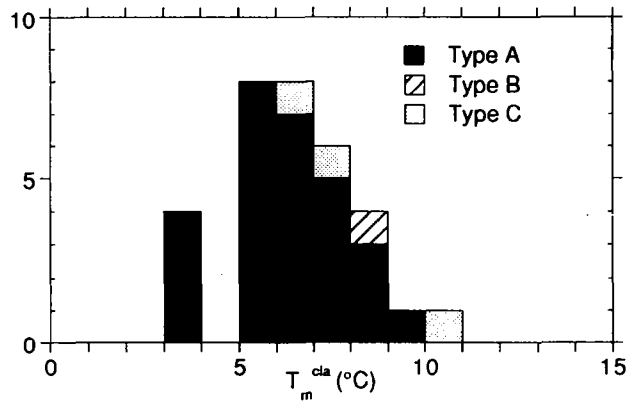

Fig. 7. Cumulative histograms of T_m^{cla}. Clathrate melting episodes in some inclusions of type B indicate the presence of a small, miscible carbonic fraction.

fluids within type B and C inclusions are easier to describe, since they can be studied in the better constrained H_2O–NaCl and CO_2–CH_4 subsystems, respectively.

The composition of type A inclusions was estimated using the computer program FLINCOR (Brown, 1989). The approach consists of defining first the molar fraction of methane in the carbonic phase, on the basis of $T_m^{CO_2}$ and $T_h^{CO_2}$, then the salinity of the aqueous phase as a function of either T_m^{cla} or T_m^{ice}, and finally the bulk inclusion fractions and density on the basis of the estimated vol.% H_2O. Quantitative uncertainties affect the method in each of the above points. X_{CH_4} is typically determined by the graphic approaches of Hollister & Burruss (1976), Heyen *et al.*, (1982) or Swanenberg (1979), which are strictly applicable only to H_2O-free fluids. If water (and hence clathrate) is present, errors arise because of the differential partitioning of carbonic species among the carbonic fluid and clathrate (Seitz *et al.*, 1987; Dubessy *et al.*, 1989), and because of the effects of clathrate on the volumetric properties of the fluid (Heyen *et al.*, 1982; Ramboz *et al.*, 1985). As a result, it is not uncommon (Seitz & Pasteris, 1990; this study) to measure $T_m^{CO_2}$ and $T_h^{CO_2}$ values which do not intersect in the v–X diagram proposed by Heyen *et al.* (1982). According to Seitz *et al.* (1987), the difference between the CO_2/CH_4 ratio of the bulk fluid and that of the residual carbonic fraction can be noticeable, and generally results in an underestimate of the bulk methane content. In the present study, the effects of enclathration on CH_4/CO_2 have been ignored, and the method of Heyen *et al.* (1982) applied. As a consequence, mean values of X_{CH_4} of about 0.15, with a minimum of 0.04 for sample VR650 and a maximum of 0.35 for VR498b2, are considered representative of the carbonic fraction of type A inclusions.

Accurate determination of the bulk salinity (expressed in terms of 'equivalent' NaCl: $NaCl_{eq}$) is also difficult for inclusions in the full C–O–H–NaCl system, again because of the presence of clathrate that prevents use of T_m^{ice} depression. Use of the depression of T_m^{cla}, as suggested by Collins (1979) or Diamond (1992), is also problematic, since the presence of CH_4 in the clathrate counteracts the effects of dissolved salts (Hollister & Burruss, 1976). As an example, consider an inclusion from sample VR489b1, not

listed in Table 2, that has $T_m^{ice} = -8.3°$ C and $T_m^{cla} = 8°$ C; this inclusion has an estimated X_{CH_4} of 0.12 in the carbonic fraction. If the depression of T_m^{ice} is considered, a salinity of 13 wt% $NaCl_{eq}$ is determined, whereas T_m^{cla} gives <4% in the methane-absent system (Diamond, 1992; Fig. 5). Taking into consideration that 12% CH_4 has the effect of raising T_m^{cla} by about 1° C (Hollister & Burruss, 1976), a bulk salinity of about 6 wt% $NaCl_{eq}$ in the aqueous fraction is deduced (Collins, 1979; Diamond, 1992). Given the ranges of T_m^{ice}, T_m^{cla} and X_{CH_4}, we can conclude that type A inclusions have a low salinity, generally <10 wt% $NaCl_{eq}$. The presence of the additional compounds CH_4 and salt is responsible for the expansion of the H_2O–CO_2 solvus to temperatures in excess of 335° C, as indicated by the measured T_h^f of type A inclusions.

In the case of type B inclusions, salinity can be simply determined as a function of depression of T_m^{ice}, that indicates salinities lower than 15 wt% $NaCl_{eq}$. The bulk salinity of type B inclusions is systematically higher than the apparent bulk salinity of type A from the same sample (Table 2).

Bulk density and methane content of type C inclusions have been calculated with the method of Heyen *et al.* (1982), because these inclusions are water-free: type C inclusions are CO_2–CH_4 mixtures with up to 25 mol.% CH_4. The methane fraction of these fluids is (except for the extreme compositions of sample VR489b2) the same as in the carbonic fraction of coexisting type A inclusions: in fact inclusion types A and C typically overlap in the $T_m^{CO_2}$ vs. $T_h^{CO_2}$ of Fig. 5. Although the methane content is almost constant in each sample, there are significant density variations within type C inclusions, as reflected by changes in $T_h^{CO_2}$. This is also the case in type A inclusions (lower $T_m^{CO_2}$ indicates higher densities). Note that the calculated composition of type C inclusions is not stable at any P–T condition of geological interest (Holloway, 1984; Lamb & Valley, 1985; Kreulen, 1987) and as a consequence cannot be indicative of a primary fluid. Such a conclusion would still be valid even if a small, optically undetectable amount of water was present in the inclusions as suggested by the rare clathrate or ice melting episodes. The significance of CO_2–CH_4 inclusions is discussed in the following section.

Isochores have been obtained for the three inclusion types using the computational option of FLINCOR (Fig. 8a,b) and the equations of state of Kerrick & Jacobs (1981) for carbonic inclusions, and of Bowers & Helgeson (1983) for aqueous-saline fluids.

FLUID EVOLUTION WITH *P–T–* DEFORMATION HISTORY

The consistency of microstructural, compositional and volumetric data in all studied samples allows reconstruction of the evolutionary history of fluid inclusions during (?) and after the genesis of the andalusite-bearing veins. The reconstruction takes into account that: (1) contact metamorphism and vein formation took place at pressures between 2.5 and 3.7 kbar, starting from temperatures of 350 ± 50° C; (2) graphite appears to be present within

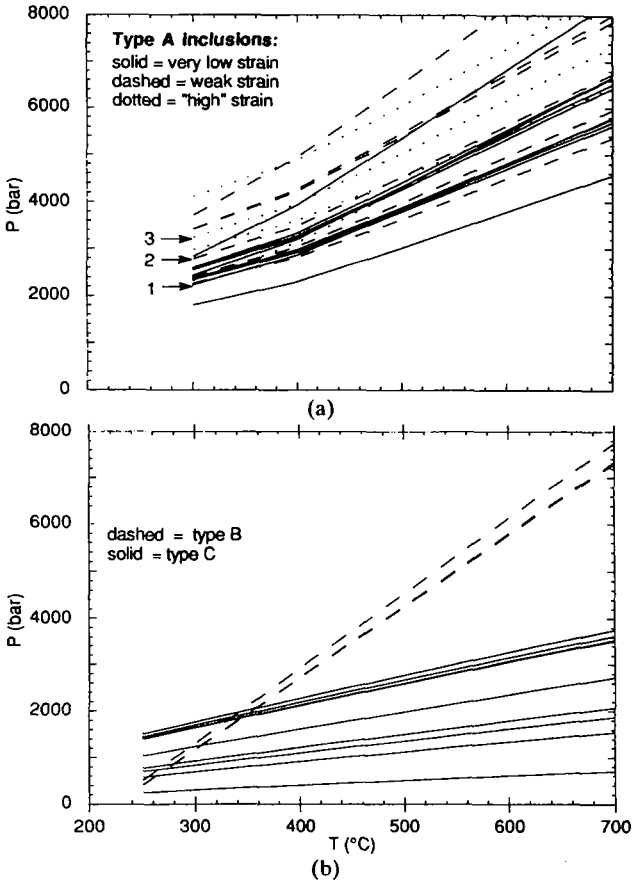

Fig. 8. (a) Representative isochores for type A inclusions, distinguished on the basis of petrographic evidence of strain. Arrows indicate isochores obtained from the three type A inclusions of sample VR471, listed in Table 2. (b) Representative isochores for type B and C inclusions.

many carbonic inclusions of both type A and type C; and (3) host quartz grains show various degrees of internal strain.

Aqueous and water-free carbonic inclusions (types B and C) cannot be considered representative of fluids present at the time of vein formation: type B inclusions are always confined to late planes and trails that cross-cut grain boundaries, and CO_2–CH_4 mixtures such as those present in type C inclusions are not stable at any P–T conditions. As a consequence, only the H_2O–CO_2–CH_4–NaCl inclusions of type A can possibly contain a primary fluid.

Type A inclusions are water-rich carbonic mixtures with low salinity. Their estimated $CH_4/(CH_4 + CO_2)$ ratio varies from 0.04 to 0.35, but is quite constant in each sample. The main parameter that causes the variability of type A inclusions is density, which shows relevant changes within each sample (Table 2), and determines the range of isochores. As shown in Fig. 8(a), in particular for the labelled inclusions of sample VR471, density changes can be related to different strain conditions of the host quartz: inclusions within optically unstrained grains have the lowest densities (the highest $T_h^{CO_2}$), and there is a progressive increase in density through the weakly strained

areas (weak undulose extinction) up to the highly strained grains. We also observed, as did Kerrich (1976), that recrystallized grains have no aqueous fluid inclusions. Thus, we can infer that post-entrapment, ductile deformation of quartz produced a progressive increase in the density of type A inclusions; this suggests conditions of decreasing temperature (in an isobaric regime) during re-equilibration of the later inclusions. The possible 'early' fluids, trapped during vein formation, should then be recognized in the inclusions with the highest $T_h^{CO_2}$, which form well-defined clusters in the $T_m^{CO_2}$ vs. $T_h^{CO_2}$ diagram of Fig. 5. Remnant type A inclusions, with lower $T_m^{CO_2}$, probably formed during strain-assisted change in volume of the inclusions and re-equilibration of the fluid at lower temperatures. The effect of strain on fluid density is apparent in the andalusite-rich vein VR650 (Fig. 5). Here, although single grains of host quartz are completely embedded within andalusite, strain partitioning in the matrix external to the andalusite was prevented, and the whole vein aggregate was weakly, but homogeneously, deformed.

Since the bulk composition of type A inclusions is quite constant in each sample, we can assume the re-equilibration process occurred when the fluid was still miscible (i.e. above 330° C, the average observed T_h^f), and without leakage of components. Leakage might have occurred only in those type A inclusions that homogenize to the vapour phase.

The P–T conditions and timing of entrapment are more difficult to derive for the metastable type C carbonic inclusions. On the basis of $T_h^{CO_2}$ we deduce that their density is similar or higher than the carbonic fraction of the reworked type A inclusions, with which they are texturally associated. Equilibrium behaviour of type C inclusion fluids requires them to re-speciate, with the production of H_2O and graphite by the reaction

$$CO_2 + CH_4 = 2H_2O + 2C,$$

until a water-rich fluid is obtained. Obviously, such reaction has not occurred in inclusion type C, and the likely explanation is failure in the nucleation of graphite. These kinetic barriers are particularly effective at low temperature (<300–400° C, Hall & Bodnar, 1990), so that genesis of CO_2–CH_4 inclusions may only be a low-T phenomenon. Considering that T_h^f values indicate the unmixing of the complex C–O–H–NaCl fluids of type A inclusion at temperatures around 330° C, a very likely origin of type C inclusions is the trapping of the carbonic fraction of unmixed type A fluids. Under such circumstances, the low temperature would not allow the fluid to re-speciate.

The proposed genetic relationship between type A and C fluids is strongly supported by: (a) their similar textural occurrence and strain/density relationships, (b) their almost identical CO_2/CH_4 ratios and (c) the presence of dark coatings of graphite on the walls of many inclusions of both types. Because graphite is more likely to be a daughter mineral than a solid inclusion, its presence within the H_2O-free type C inclusions implies H_2O was indeed present in a former fluid (i.e. an inclusion of type A), and was subsequently removed after unmixing, either by complete re-opening of the inclusion or by selective migration (wicking, e.g. Crawford & Hollister, 1986).

The salinity of type B inclusions shows a slight increase when compared to type A (Table 2), again suggesting a genetic link among this inclusion generation and the 'early', type A fluids. In fact, the salinity increase is consistent with type B inclusions representing the H_2O-rich fraction separated after low-T unmixing of the former H_2O–CO_2–CH_4–NaCl fluid. In this case, the shape of the $(CO_2 + CH_4)$–$(H_2O + NaCl)$ solvus predicts that a small carbonic fraction should still be miscible on the H_2O-rich side: the episodes of clathrate melting observed in a few of the type B inclusions support this hypothesis. However, the microstructural evidence suggests that type B and C inclusions were trapped at different times, rather than simultaneously from a boiling fluid. An alternative interpretation is that type B inclusions contain a fluid genetically unrelated to the carbonic generation A. Such aqueous fluid of unknown origin would have been present in the rock samples at some stage during their exhumation and cooling.

DISCUSSION

The main points of this study are (1) the relationships defined between the veining episode and formation of the fluid inclusions and (2), for the 'primary' inclusions recognized, the direct observation of fluids capable of transport and concentration of 'immobile' aluminium in the vein andalusite.

Because microstructures and composition/density data indicate that the lowest density type A inclusions most likely represent the vein-filling fluids, this study allows discussion of an important assumption of the synmetamorphic veining model proposed by Cesare (1994a): if veins formed as a result of dehydration of graphitic metapelites, the fluid would be a C–O–H mixture in equilibrium with graphite. Being the product of re-speciation of graphite and water, the fluid should have an X_O ratio [$O/(O + H)$, Connolly & Cesare, 1993; Connolly, 1995] of 1/3, and a carbonic fraction comprising equal molar amounts of CO_2 and CH_4 (Ohmoto & Kerrick, 1977). The maximum estimated $CH_4/(CH_4 + CO_2)$ of type A inclusions is about 0.35, and X_O ranges from 0.37 to 0.50. When the inclusion with the lowest X_O ratio (0.37 in sample VR357) is considered, its compositional and volumetric properties, determined on the basis of microthermometric data, almost coincide with values calculated (Table 3) as a

Table 3. Composition of a representative type A fluid inclusion from sample VR357 (inclusion n. 1 in Table 2), estimated from microthermometric data, compared with calculated speciation of a fluid with same X_O (0.37) in equilibrium with graphite at 3.5 kbar, 600° C. *Fluid speciation calculated with the method of Connolly (1995; appendix 1).

	Estimated	Calculated*
X_O	0.37	0.37
X_{H_2O}	0.86	0.87
X_{CO_2}	0.10	0.11
X_{CH_4}	0.02	0.03

function of X_O, T and P at peak metamorphic conditions (a temperature of 600° C has been used in this case, since this sample belongs to the higher-grade zone of outcrop 2). This inclusion also provides an isochore passing very close to the andalusite stability field. Although these data strengthen the hypothesis of a primary origin for at least some type A inclusions, they also indicate that the fluid was not simply the product of dehydration of a graphitic pelite, as predicted by the veining model, but also comprised some CO_2 in excess (8–30 mol%). This CO_2 fraction must have been present within the metapelites during dehydration and veining, either as an external fluid or as carbonic fluid inclusions reworked by metamorphism.

A problem concerns the P–T location of isochores calculated for such 'early' fluids: except for two inclusions, isochores do not intersect the andalusite stability field (as defined by Holdaway & Mukophadyay, 1993), but pass at slightly higher pressures. In particular, isochores for inclusions in unstrained host quartz (solid lines in Fig. 8a) are located up to 1 kbar off the maximum pressure of andalusite stability. Because all geological and petrological data indicate that veins formed in the stable presence of andalusite (Cesare, 1994a), the location of isochores would suggest that not even type A fluids can be considered 'primary'. However, it must be recalled that extrapolation at metamorphic conditions of isochores in the complex C–O–H–NaCl system is impeded by errors due to the visual estimate of vol.% H_2O (Burruss, 1981), and by uncertainties related to the scarce experimental data. The estimated vol.% H_2O of type A inclusions ranges from 30 to 60, and corresponds to $X_{H_2O} = 0.52$–0.86 in the bulk fluid (Table 2). Owing to the irregular shape and small size of many of the inclusions, visual estimates of vol.% H_2O can have large uncertainties. For example, correction of −10 vol.% H_2O in type A inclusions would move isochores to lower pressures (≈ 500 bar at 500° C), and then most of them would cross the andalusite stability field. Furthermore, recent improvement of the v–X properties of the CO_2–CH_4 binary system (Thiéry *et al.*, 1994) have revealed the systematic overestimation of the molar volume of the liquid carbonic phase introduced in the v–X diagram of Heyen *et al.* (1982). Also, this error results in pressure overestimates (only for isochores of type A inclusions) of the order of a few hundred bar.

Because of the possibility of systematic errors in their real location, isochores passing at pressures slightly higher than the predicted P–T conditions of vein formation are not sufficient to invalidate the interpretation of an 'early' origin for some of the type A inclusions. Hence, considering all the quantitative uncertainties in their actual P–T position, we conclude that isochores of type A inclusions support the model that rock failure and veining took place in a regime of lithostatic fluid pressure.

The reliability of isochores for barometric purposes and the reconstruction of composition of palaeo-fluids are typically based on the assumption that no chemical or density changes occurred after fluid inclusion entrapment. In contrast, we have shown that strain-assisted increase in density is likely to have affected some of the type A inclusions. Chemical changes (e.g. the possibility of diffusion in and out of fluid inclusions) are also proposed to explain differences between theoretical and calculated fluid compositions (Roedder & Skinner, 1968; Bakker & Jansen, 1994). Recently, particular attention has been paid to the diffusion of hydrogen (e.g. Hall & Bodnar, 1990; Morgan *et al.*, 1993), and experimental studies in the system C–O–H have demonstrated how this process can actually modify bulk fluid compositions. If hydrogen diffusion out of type A inclusions had occurred, it would explain the observed departure of X_{CH_4} from the model value of 0.5 (corresponding to $X_O = 1/3$). However, there is no evidence for postulating such a phenomenon, since differences in fluid compositions and densities within single textural sites are preserved.

Textures and microthermometry provide a coherent history of the evolution of fluid inclusions within the andalusite-bearing veins that can be integrated with independently obtained P–T–t data on vein host-rocks. The proposed P–$T(-t)$ path from Oligocene to present (Fig. 9) shows a first heating–cooling stage related to the emplacement of the intrusive (sector 1–2/2′ to 3 in Fig. 9), followed by a cooling and exhumation trajectory (sector 3–4) that is only constrained by data on apatite fission tracks (Grundmann & Morteani, 1985). The heating–cooling pulse of contact metamorphism, which starts from a metamorphic temperature of 350° C (point 1), is not strictly isobaric. In fact, assuming a constant exhumation rate of 0.3 mm/yr (Cesare, 1992), heat conduction models (Peacock, 1989) predict a minimum decompression of 0.5 kbar before rocks located within 800 m of the contact (a thickness that encompasses both vein outcrops) cool down to temperatures lower than 350° C (point 3). Since heating takes place faster than cooling, the decompression has been mostly attributed to the retrograde path. The prograde path of contact metamorphism has been extended within the sillimanite stability field up to 600° C (point 2′), to account for the presence of coarse sillimanite after andalusite in rocks from outcrop 2. After trapping of the early type A fluids during vein formation in the andalusite stability field, ductile strain of inclusions under decreasing temperature caused the complex C–O–H–NaCl mixtures to re-equilibrate. Since the cooling trajectory is flatter than isochores of type A fluids, a progressive increase in inclusion density occurred. This process probably took place until rocks cooled to temperatures of about 350–400° C, and was accompanied by precipitation of graphite within inclusions. Further temperature decrease caused the unmixing of type A fluids: the metastable type C inclusions are likely to have formed at these low-T conditions, by removal of the H_2O-rich fraction. Aqueous type B inclusions may have been trapped at the same time, as the intersection of their isochores could indicate, but they are more likely to be younger, as denoted by the microstructural analysis. Sector 3–4 in the P–$T(-t)$ path of Fig. 9 has been drawn to allow both possibilities. Since aqueous inclusions have homogenization temperatures of about 225° C, inclusion types B and C are believed to have formed in the interval 225–350° C

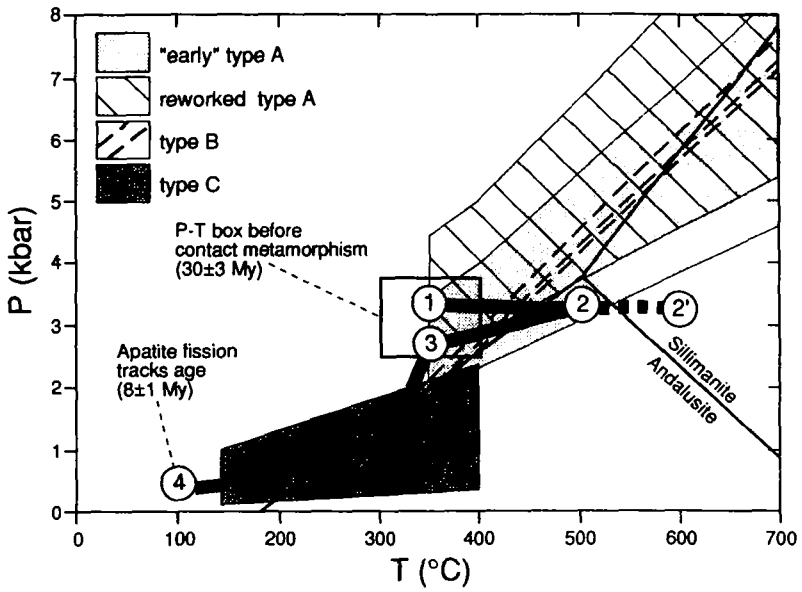

Fig. 9. Possible P–T(–time) path, marked by the thick line, for the andalusite-bearing veins and adjacent host-rocks in the southern Vedrette di Ries aureole. Al_2SiO_5 triple point after Holdaway & Mukophadyay (1993). Type A isochores drawn for T > 350° C to allow trapping of a miscible fluid; isochores for metastable type C fluids drawn for T < 400° C, assuming a low-T genesis (see text for discussion). Temperature of points 1 and 4 is time-constrained by radiometric data (Borsi *et al.*, 1979; Grundmann & Morteani, 1985; respectively). The dashed part of the path (3–4) has been drawn to allow trapping of type C inclusions before or together with type B. A decompression of about 0.6 kbar has been attributed to the heating–cooling pulse of contact metamorphism (1–2/2' to 3). Pressure at point 4 was assumed arbitrarily.

(i.e. at conditions overlapping the boundary for cataclastic/plastic behaviour of quartz). Selective preservation of the carbonic fraction of unmixed fluids is consistent with the relationships between deformation and fluid trapping proposed by Hollister (1990) and Johnson & Hollister (1995).

CONCLUSIONS

All available information suggest that the isolated, lowest density, H_2O–CO_2–CH_4–NaCl type A inclusions are representative of the fluids present during vein formation. The composition and density of these 'primary' inclusions are consistent with a C–O–H fluid in equilibrium with graphite at the estimated P–T conditions of veining, and with a regime of lithostatic fluid pressure during crystallization of vein minerals. The low salinity of the aqueous fraction indicates that increased solubility in 'aggressive' fluids (e.g. Kerrick, 1990) is not required for effective aluminium transport. Hence, the synmetamorphic veining model, proposed for the andalusite-bearing veins of the Vedrette di Ries aureole by Cesare (1994a), is supported by the study of fluid inclusions.

The reconstruction of the P–T–deformation evolution of type A fluid inclusions documents an increase in density at constant composition that occurred during quasi-isobaric cooling from peak metamorphic temperature to the starting value of *c.* 350° C. The density changes are variously recorded in each sample as a function of the degree of strain and of the relative abundance of quartz and andalusite.

This research also provides an overall indication of the behaviour of C–O–H fluids during metamorphism and subsequent cooling and exhumation of rocks: in particular, it is important to consider that constant-mass, down-temperature re-equilibration should cause graphite precipitation within inclusions, as well as changes in the primary $H_2O/CO_2/CH_4$ fluid proportions. From this perspective, careful investigation for the presence of graphite lining inclusion walls is essential. Furthermore, the inferred genetic relationships between different inclusion types from this study indicate that, when strain occurs, the bulk composition of fluids is likely to be radically modified after entrapment of primary inclusions, so that room-temperature composition–volume data may provide erroneous information on fluids present at the time of metamorphism. Hence, fluid inclusion data need to be integrated with detailed field, microstructural and petrographic investigations, in order to use them for meaningful reconstruction of fluid evolution and for recognition of possible primary fluids.

ACKNOWLEDGEMENTS

The project was supported by NSF grant EAR 90-04573 to L.S.H., by Italian MURST 40%, and by a scholarship from foundation 'Gini' of the University of Padova (to B.C.). We thank D. Johnson for providing excellent doubly polished thick sections, C. Brogiato for help with inclusion photography and D. Winslow for Raman analyses. We also thank the organizers and participants at the Summer School at Siena, Italy, for providing a stimulating environment within which this collaboration began. Careful reviews by P. Brown, P. Philippot and J. Selverstone improved the manuscript and were very much appreciated.

REFERENCES

Bakker, R. J. & Jansen, B. H., 1994. A mechanism for preferential H_2O leakage from fluid inclusions in quartz, based on TEM observations. *Contributions to Mineralogy and Petrology*, **116**, 7–20.

Becker, L. P., Frank, W., Höck, V., Kleinschmidt, G., Neubauer, F., Sassi, F. P. & Schramm, J. M., 1987. Outlines of the pre-Alpine metamorphic events in the Austrian Alps. In: *Pre-Variscan and Variscan Events in the Alpine-Mediterranean Mountain Chains* (eds Flügel, H. W., Sassi, F. P. & Grecula, P.), pp. 69–106. Alfa Publisher, Bratislava.

Borsi, S., Del Moro, A., Sassi, F. P., Zanferrari, A. & Zirpoli, G., 1978. New petrologic and radiometric data on the Alpine history of the Austridic continental margin south of the Tauern Window (eastern Alps). *Memorie di Scienze Geologiche*, **32**, 1–20.

Borsi, S., Del Moro, A., Sassi, F. P. & Zirpoli, G., 1979. On the age of the Vedrette di Ries (Rieserferner) massif and its geodynamic significance. *Geologische Rundschau*, **68**, 41–60.

Bowers, T. S. & Helgeson, H. C., 1983. Calculation of the thermodynamic and geochemical consequences of nonideal mixing in the system H_2O–CO_2–NaCl on phase relations in geologic systems: metamorphic equilibria at high pressures and temperatures. *American Mineralogist*, **68**, 1059–1075.

Brown, P. E., 1989. FLINCOR: a microcomputer program for the reduction and investigation of fluid-inclusion data. *American Mineralogist*, **74**, 1390–1393.

Burruss, R. C., 1981. Analysis of fluid inclusions: phase equilibria at constant volume. *American Journal of Science*, **281**, 1104–1126.

Cesare, B., 1992. Metamorfismo di contatto di rocce pelitiche nell'aureola di Vedrette di Ries (Alpi Orientali). *Unpubl. PhD Thesis, Padova University*.

Cesare, B., 1994a. Synmetamorphic veining: origin of andalusite-bearing veins in the Vedrette di Ries contact aureole, Eastern Alps, Italy. *Journal of Metamorphic Geology*, **12**, 643–653.

Cesare, B., 1994b. Hercynite as the product of staurolite decomposition in the contact aureole of Vedrette di Ries, eastern Alps, Italy. *Contributions to Mineralogy and Petrology*, **116**, 239–246.

Collins, P. L. F., 1979. Gas hydrates in CO_2-bearing fluid inclusions and the use of freezing data for estimation of salinity. *Economic Geology*, **74**, 1435–1444.

Connolly, J. A. D., 1995. Phase diagram methods for graphitic rocks and application to the system C–O–H–FeO–TiO_2–SiO_2. *Contributions to Mineralogy and Petrology*, **119**, 94–116.

Connolly, J. A. D. & Cesare, B., 1993. C–O–H–S Fluid composition and oxygen fugacity in graphitic metapelites. *Journal of Metamorphic Geology*, **11**, 379–388.

Crawford, M. L. & Hollister, L. S., 1986. Metamorphic fluids: the evidence from fluid inclusions. In: *Fluid-Rock Interactions During Metamorphism* (eds Walther, J. W. & Wood, B.J.), pp. 1–35. Springer-Verlag, New York.

Diamond, L. W., 1992. Stability of clathrate hydrate + CO_2 liquid + CO_2 vapour + aqueous KCl-NaCl solutions: experimental determination and application to salinity estimates of fluid inclusions. *Geochimica et Cosmochimica Acta*, **56**, 273–280.

Dubessy, J., Poty, B. & Ramboz, C., 1989. Advances in C–O–H–N–S fluid geochemistry based on micro-Raman spectrometric analysis of fluid inclusions. *European Journal of Mineralogy*, **1**, 517–534.

Frank, W., Kralik, M., Scharbert, S. & Thöni, M., 1987. Geochronological data from the eastern Alps. In: *Geodynamics of the Eastern Alps* (eds Flügel, H. W. & Faupl, P.), pp. 272–281. Deuticke, Wien.

Grundmann, G. & Morteani, G., 1985. The young uplift and thermal history of the central Eastern Alps (Austria, Italy), evidence from apatite fission tracks ages. *Jahrbuch Geologie BA*, **128**, 197–216.

Hall, D. L. & Bodnar, R. J., 1990. Methane in fluid inclusions from granulites: a product of hydrogen diffusion? *Geochimica et Cosmochimica Acta*, **54**, 641–651.

Heyen, G., Ramboz, C. & Dubessy, J., 1982. Simulation des equilibres de phase dans le systeme CO_2–CH_4 en dessous de 50° C et de 100 bar. Application aux inclusions fluides. *Comptes Rendus Academie Sciences, Paris*, **294**, 203–206.

Holdaway, M. J. & Mukhopadhyay, B., 1993. A reevaluation of the stability relations of andalusite: thermochemical data and phase diagram for the aluminum silicates. *American Mineralogist*, **78**, 298–315.

Hollister, L. S., 1990. Enrichment of CO_2 in fluid inclusions in quartz by removal of H_2O during crystal-plastic deformation. *Journal of Structural Geology*, **12**, 895–901.

Hollister, L. S. & Burruss, R. C., 1976. Phase equilibria in fluid inclusions from the Kthada Lake metamorphic complex. *Geochimica et Cosmochimica Acta*, **40**, 163–175.

Holloway, J. R., 1984. Graphite–CH_4–H_2O–CO_2 equilibria at low-grade metamorphic conditions. *Geology*, **12**, 455–458.

Johnson, E. L. & Hollister, L. S., 1995. Syndeformational fluid trapping in quartz: determining the pressure–temperature conditions of deformation from fluid inclusions and the formation of pure CO_2 fluid inclusions during grain boundary migration. *Journal of Metamorphic Geology*, **13**, 239–249.

Kerrich, R., 1976. Some effects of tectonic recrystallization on fluid inclusions in vein quartz. *Contributions to Mineralogy and Petrology*, **59**, 195–202.

Kerrick, D. M., 1988. Al_2SiO_5-bearing segregations in the Lepontine Alps, Switzerland: aluminum mobility in metapelites. *Geology*, **16**, 636–640.

Kerrick, D. M., 1990. The Al_2SiO_5 polymorphs. *Reviews in Mineralogy*, **22**. Mineralogical Society of America, Washington, DC.

Kerrick, D. M. & Jacobs, G. K., 1981. A modified Redlich-Kwong equation of state for H_2O, CO_2, and H_2O–CO_2 mixtures at elevated pressure and temperatures. *American Journal of Science*, **281**, 735–767.

Kreulen, R., 1987. Thermodynamic calculations of the C–O–H system applied to fluid inclusions: are fluid inclusions unbiassed samples of ancient fluids? *Chemical Geology*, **61**, 59–64.

Mager, D., 1985. Geologische und petrographische untersuchungen am Südrand des Rieserferner-Plutons (Südtirol) unter Berücksichtigung des Intrusionsmechanismus. *Unpubl. PhD Thesis, Erlangen University*.

Morgan, G.B. VI, I-Ming Chou, Pasteris, C. & Olsen, S. N., 1993. Re-equilibration of CO_2 fluid inclusions at controlled hydrogen fugacities. *Journal of Metamorphic Geology*, **11**, 155–164.

Ohmoto, H. & Kerrick, D., 1977. Devolatilization equilibria in graphitic systems. *American Journal of Science*, **277**, 1013–1044.

Peacock, S. M., 1989. Thermal modeling of pressure-temperature-time paths: a forward approach. In: *Metamorphic Pressure-Temperature-Time Paths* (eds Spear, F. S. & Peacock, S.M.), pp. 1–55. Short course in geology, American Geophysical Union.

Ramboz, C., Schnapper, D. & Dubessy, J., 1985. The P–V–T–X–f_{O2} evolution of H_2O–CO_2–CH_4-bearing fluid inclusions in a wolframite vein: reconstruction from fluid inclusion data. *Geochimica et Cosmochimica Acta*, **49**, 205–219.

Roedder, E., 1979. Fluid inclusions as samples of ore fluids. In: *Geochemistry of Hydrothermal Ore Deposits* (ed. Barnes, H.L.), pp. 515–574. Wiley, New York.

Roedder, E., 1984. Fluid Inclusions. *Reviews in Mineralogy*, Vol. 12. Mineralogical Society of America, Washington, DC.

Roedder, E. & Skinner, B. J., 1968. Experimental evidence that fluid inclusions do not leak. *Economic Geology*, **63**, 715–730.

Seitz, J. C. & Pasteris, J. D., 1990. Theoretical and practical apects of differential partitioning of gases by clathrate hydrates in fluid inclusions. *Geochimica et Cosmochimica Acta*, **54**, 631–639.

Seitz, J. C., Pasteris, J. D. & Wopenka, B., 1987. Characterization of CO_2–CH_4–H_2O fluid inclusions by microthremometry and laser Raman microprobe spectroscopy: inferences for clathrate and fluid equilibria. *Geochimica et Cosmochimica Acta*, **51**, 1651–1664.

Stöckhert, B., 1982. Deformation und retrograde Metamorphose im Altkristallin S' des westlichen Tauernfensters (Südtirol). *Unpubl. PhD Thesis, Erlangen University*.

Swanenberg, H. E. C., 1979. Phase equilibria in carbonic systems,

and their application to freezing studies of fluid inclusions. *Contributions to Mineralogy and Petrology*, **68**, 303–306.

Thiéry, R., Van den Kerkhof, A. M. & Dubessy, J., 1994. vX properties of CH_4–CO_2 and CO_2–N2 fluid inclusions: modelling for $T < 31°C$ and $P > 400$ bars. *European Journal of Mineralogy*, **6**, 753–771.

Yardley, B. W. D., 1986. Fluid migration and veining in the Connemara schists, Ireland. In: Fluid-Rock Interaction During Metamorphism (eds Walther, J. V. & Wood, B. J.), *Advances in Physical Geochemistry*, **5**, 109–131.

Received 31 August 1994; revision accepted 15 March 1995.